Real-space refinement of single-crystal electron diffuse scattering and its application to $Bi_2Ru_2O_{7-\delta}$

2007 J. Phys.: Condens. Matter 19 335216

(http://iopscience.iop.org/0953-8984/19/33/335216)

IOP PUBLISHING JOURNAL OF PHYSICS: CONDENSED MATTER

J. Phys.: Condens. Matter **19** (2007) 335216 (15pp) doi:10.1088/0953-8984/19/33/335216

Real-space refinement of single-crystal electron diffuse scattering and its application to $Bi_2Ru_2O_{7-\delta}$

A L Goodwin[1], R L Withers[2] and H-B Nguyen[2]

[1] Department of Earth Sciences, University of Cambridge, Downing Street, Cambridge CB2 3EQ, UK
[2] Research School of Chemistry, Australian National University, Canberra, ACT 0200, Australia

E-mail: withers@rsc.anu.edu.au

Received 1 March 2007, in final form 2 March 2007
Published 4 July 2007
Online at stacks.iop.org/JPhysCM/19/335216

Abstract

A real-space atomistic refinement approach to the analysis of experimental electron diffraction patterns is described. The method employs the reverse Monte Carlo algorithm to produce atomistic configurations capable of qualitatively reproducing diffuse electron scattering patterns. Its implementation in the program EDRMC is described in detail, together with a number of additional constraints/restraints that can be used to guide the refinement process. In particular, appropriate restraints ensure the individual atomic displacements introduced to model the diffuse scattering patterns are simultaneously consistent with the known average structure. The approach is then used to interpret electron diffraction patterns measured for $Bi_2Ru_2O_{7-\delta}$. The diffuse scattering patterns observed are shown to arise primarily from concerted translations of Bi atoms. These translations can be interpreted in terms of rotations of $[O'Bi_4]$ tetrahedra correlated along the $\langle 110 \rangle$ crystal axes and uncorrelated along orthogonal directions.

(Some figures in this article are in colour only in the electronic version)

1. Introduction

Electron diffraction is well established as a method of choice for the experimental determination of single-crystal structured diffuse scattering patterns [1]. Similar information can of course be measured using x-rays or neutrons, but electron diffraction—while only semi-quantitative—boasts the advantages of increased diffuse intensity, ready accessibility and the routine ability to focus on very small crystallites (around 0.5 μm). The geometry and relative intensities of the diffuse scattering patterns so determined invariably contain valuable information regarding disorder in crystalline materials—whether compositional or displacive, dynamic or static [2–7]. While it is a relatively straightforward process to calculate the diffuse scattering one expects for a system where the mechanism of disorder is already known, the *inverse* exercise of deducing the type of disorder from a given diffuse scattering pattern is in general far from trivial. And

yet understanding crystalline disorder is key to appreciating a wide range of important physical behaviours, including high-T_c superconductivity [8], colossal magnetoresistance [9], solid-state ion transport [10], negative thermal expansion [11] and the existence of phase transitions [12] and unusual electronic properties [13]. Certainly, recognisable general trends do emerge: particular patterns of diffuse scattering will often be associated with the same general processes across broad structural families [1]. However, there is a strong drive to develop methods of analysing diffuse scattering patterns in more general terms, in an effort to understand disorder in increasingly diverse systems.

One approach is to use atomistic simulation methods, such as the Monte Carlo approach, to 'test' possible disorder mechanisms for a given system of interest [4]. An appropriate interaction potential (or ensemble of potentials) is used to drive the simulation, and then diffuse scattering patterns are calculated from the refined equilibrium configurations. Since one is generally interested primarily in the form of the potential rather than the precise values of its various parameters, only qualitative similarity between the calculated and observed diffuse scattering patterns is ever demanded. In many instances this approach yields very satisfactory results, particularly when applied in conjunction with a sound knowledge of crystal chemistry. However, there always remains the inherent presupposition of a particular disorder mechanism, and so the approach is of more limited use whenever an appropriate mechanism is not known *a priori*. This limitation can be circumvented somewhat by iterative refinement of the form of the potential itself—an approach implemented with obvious success in the EPSR method, designed for use with one-dimensional diffraction data (such as collected from powders, liquids or amorphous materials) [14]. While similar approaches have been proposed for single-crystal calculations, the sheer magnitude of computation involved has generally proven prohibitive [15].

The reverse Monte Carlo (RMC) approach [16] would seem to offer a particularly attractive alternative, since its refinement of atomistic models is driven by experimental data rather than by pre-determined interaction potentials. Indeed RMC-based methods for refining structural models against single-crystal neutron [17] and x-ray [18–20] diffuse scattering patterns have been reported previously, and have been shown capable of providing reliable information regarding occupational and displacement correlations. The extension to refinement of electron diffraction data follows rather straightforwardly, and it is perhaps surprising that its use appears not to have been reported (other than for orientationally averaged data—see, for example [21]). The relative ease with which high-quality electron diffraction images can be obtained for multiple sections of reciprocal space, and the capacity to measure single-crystal data from polycrystalline samples, are both strongly motivating factors for the development of an electron diffraction RMC (EDRMC) approach.

In this paper we describe such an approach for producing real-space atomistic configurations consistent with electron diffuse scattering patterns, and outline some methods for interpreting these configurations in terms of the underlying processes responsible for the observed diffuse scattering. We apply this technique to the pyrochlore $Bi_2Ru_2O_{7-\delta}$ and show that the structured diffuse scattering observed for this material can be attributed to correlated rotations of one-dimensional chains of $[OBi_4]$ tetrahedra. In the process of this case study we identify some limitations in the proposed approach and highlight aspects where particular care must be taken in order to avoid the generation of spurious results.

2. EDRMC implementation

2.1. Overview

The basic structure of our EDRMC method is common to many such approaches, notably including the RMCPOW [22, 23], RMCProfile [24] and RMC++ [25] programs. A

configurational box, containing a large collection of atoms and subject to periodic boundary conditions, represents a crystallographic supercell of the material in question. Atoms within this configuration are iteratively selected and then moved at random so as to minimize the value of an 'overall mismatch function' $\chi^2_{\rm tot}$, which measures the degree to which the configuration deviates from a set of ideal parameters (fits to data, constraints and/or restraints), weighted appropriately. Proposed moves are accepted or rejected according to the Metropolis Monte Carlo algorithm until the value of χ^2 has converged, when the system is said to be at equilibrium. Equilibrium configurations are not unique but share the same overall similarity to the data and/or restraints applied.

In developing the EDRMC method, we have been forced to address the difficult issue of quantifying intensities in electron diffraction data. Unlike neutron and x-ray data, the placing of scattered intensities on an absolute scale is impractical for electron diffraction patterns: the data are complicated by multiple scattering effects and thickness dependence [1]. Consequently, any approach to model electron diffraction data using atomistic models cannot reasonably expect to provide quantitative agreement; nor would quantitative agreement be especially meaningful were it achieved. As such, our EDRMC approach aims only to fit electron diffraction patterns after suitable scale and offset factors have been applied to each image—the emphasis being to reproduce the observed *patterns* rather than absolute intensities.

In order to guide the refinement process and to provide some limits on the magnitude of atomic displacements in our models (which might be too weakly constrained if compared only against scattering patterns with arbitrary scale), we have implemented a number of additional constraints and/or restraints within our fitting process; these are described in greater detail below. Whether these constraints/restraints are appropriate for a given system may not always prove obvious, and some care must be taken when choosing which (if any) to enforce. The 'mismatch' associated with each term is simply added together to give the 'overall mismatch function':

$$\chi^2_{\rm tot} = \chi^2_{\rm diff} + \chi^2_{\rm BV} + \chi^2_{\rm avg}. \tag{1}$$

Here, 'diff' signifies the contribution due to any difference between calculated and observed diffuse scattering patterns, 'BV' that of bond valence sums, and 'avg' that of average structure factors. Each of these terms is discussed in more detail below.

2.2. *Diffuse scattering calculations*

Experimental diffuse scattering patterns are converted into EDRMC input data by indexing each image i to give a set of intensities $I_i(\mathbf{k})$ for the vectors $\mathbf{k}$ in some set D_i. We then use the method of Butler and Welberry [26] to calculate diffuse scattering intensities from the EDRMC configurations for comparison. In this method, intensities are calculated via the diffuse structure factors $A(\mathbf{k})$, defined as

$$A(\mathbf{k}) = \sum_j \left\{ f_j(k) \sum_\ell \exp[\mathrm{i}\mathbf{k}\cdot\mathbf{r}(j\ell)] - \langle F(k)\rangle \psi(\mathbf{k}) \right\}. \tag{2}$$

Here, $f_j(k)$ is the electron scattering form factor of each atom type j, $\langle F(k)\rangle$ the average unit cell structure factor and $\psi(\mathbf{k})$ an interference function given by

$$\psi(\mathbf{k}) = \prod_{\alpha\in\{x,y,z\}} \frac{\exp(\mathrm{i}k_\alpha N_\alpha) - 1}{\exp(\mathrm{i}k_\alpha) - 1}, \tag{3}$$

for a configuration with N_x, N_y, N_z unit cells along the three crystallographic axes. This method is ideal because it separates out from the total scattering function that component due

to the average periodicity of the configuration itself, and so provides a better comparison with the experimental diffuse scattering patterns. Moreover, it is possible to average over the diffuse scattering intensities calculated from a set of 'sub-boxes' of the overall configuration to further improve the 'smoothness' of the resultant scattering pattern.

In order to compare experimental and calculated diffuse scattering intensities effectively, it is necessary to calculate scale and offset factors s_i, o_i for each scattering image i. These are used to produce a set of modified calculated intensities $[s_i A(\mathbf{k})A^*(\mathbf{k}) + o_i]$ for comparison. The optimal values of these factors can be calculated automatically:

$$s_i = \frac{n_i \sum_{\mathbf{k}} I_i(\mathbf{k})A(\mathbf{k})A^*(\mathbf{k}) - \left[\sum_{\mathbf{k}} I_i(\mathbf{k})\right]\left[\sum_{\mathbf{k}} A(\mathbf{k})A^*(\mathbf{k})\right]}{n_i \sum_{\mathbf{k}} [A(\mathbf{k})A^*(\mathbf{k})]^2 - \left[\sum_{\mathbf{k}} A(\mathbf{k})A^*(\mathbf{k})\right]^2}, \tag{4}$$

$$o_i = \frac{1}{n_i}\left[\sum_{\mathbf{k}} I_i(\mathbf{k}) - s_i \sum_{\mathbf{k}} A(\mathbf{k})A^*(\mathbf{k})\right], \tag{5}$$

where n_i is the number of $\mathbf{k}$-points in each set D_i. The diffuse scattering 'mismatch' function is then given as the sum of squared differences over all experimental scattering patterns, weighted by the estimated standard deviation of each data set:

$$\chi^2_{\text{diff}} = \sum_i \sum_{\mathbf{k}\in D_i} \frac{|I_i(\mathbf{k}) - [s_i A(\mathbf{k})A^*(\mathbf{k}) + o_i]|^2}{\sigma_i^2}. \tag{6}$$

It is usually necessary to exclude from these calculations certain regions of the experimental diffuse scattering patterns; for example, spots due to Bragg reflections or obscured regions (such as from the beam stop). To this end, the user may designate a pixel 'excluded' by assigning it a negative intensity. EDRMC automatically ignores any such data point during its refinement process; however, it will continue to calculate an intensity from the configuration in the program output.

2.3. Distance window constraints

There is always the danger in any RMC refinement process of producing configurations in which the interatomic separations for some small percentage of atoms in the configuration carry unphysical values. Distance window constraints—as implemented in the RMCProfile method [24]—provide a mechanism of avoiding unphysical moves during RMC refinement without affecting any correlations that might exist in the configuration [27]. The program first assigns for each atom a set of neighbours (which may be empty). Also assigned are minimum and maximum interatomic separations for each pair of neighbouring atoms, defining a 'window' of allowed distances. Any move proposed during the refinement process is first checked to ensure that it would not cause the separation between neighbouring pairs to fall outside their corresponding 'distance window'. As such, the constraint acts to preserve a sense of connectivity in the configuration, without restricting too greatly the freedom of individual atoms to move in order to best fit the available data.

2.4. Bond valence restraints

One of the key analytical tools used when interpreting diffuse scattering patterns is a consideration of the crystal chemistry of the structure in question. That is, whether the coordination geometries, coordination numbers and bond lengths are appropriate for each atom in its particular oxidation state. A very useful tool in analysing structures in this way is the

notion of bond valence sums [28, 29]. These are empirical relationships that express a valence contribution v_{ij} of each bond in a structure to its length d_{ij}:

$$v_{ij} = \exp[(R_{ij} - d_{ij})/b]. \tag{7}$$

Here b is assigned a 'universal' value of 0.37 Å, and R_{ij} is an empirical parameter whose value can be obtained from appropriate tables [30]. The bond valence approach is based on an observation that the individual valence contributions for a given atom j, summed over all its neighbours i, tend to give the expected total valence V_j:

$$\sum_i v_{ij} = V_j. \tag{8}$$

It is straightforward to calculate a value of v_{ij} for each pair of neighbouring atoms in an EDRMC configuration—and hence an observed valence V'_j. This provides a mechanism of restraining atomic bond valences during RMC refinement through inclusion of a bond valence 'mismatch' term of the form

$$\chi^2_{\mathrm{BV}} = \sum_j \frac{(V'_j - V_j)^2}{\sigma_j^2}, \tag{9}$$

where σ_j is the standard deviation in bond valences tolerated for atom j.

2.5. Average structure factor restraints

One important concern when using a RMC approach to fit non-quantitative diffraction data is that there is little practical constraint on the magnitude of atomic displacements produced in the configurations. Ideally, additional data sets—in the form of x-ray or neutron scattering patterns, for example—might be combined with an electron diffraction approach to help provide some of this missing information. In this initial study, however, we have opted to include a structure factor restraint in lieu of implementing refinement against multiple types of diffraction data. This restraint involves an additional 'mismatch' term that represents the difference between calculated and expected x-ray structure factors ($F'(hkl)$ and $F(hkl)$, respectively). The former can be obtained readily from the EDRMC configuration:

$$F'(hkl) = \frac{1}{N} \sum_{j\ell} f_j^X(Q_{hkl}) \exp[\mathrm{i}\mathbf{Q}_{hkl} \cdot \mathbf{r}(j\ell)]. \tag{10}$$

Here $f_j^X(Q)$ is the x-ray scattering form factor of atom j. The relevant 'mismatch' term weights the contribution from each reflection (hkl) by the uncertainty $\sigma(hkl)$ in the expected structure factor and is given by

$$\chi^2_{\mathrm{avg}} = \sum_{hkl} \frac{\left|F'(hkl) - F(hkl)\right|^2}{|\sigma(hkl)|^2}. \tag{11}$$

While less elaborate than experimental Bragg intensity refinement [31]—or indeed Bragg profile refinement [24]—this approach has a number of important advantages. First, the average structure is usually well known prior to electron diffraction studies, and so a reliable list of expected x-ray structure factors can be produced without the need to collect additional data. Second, the calculation of structure factors from the EDRMC configuration is rapid, and so the average structure can be restrained without significant additional computational cost. Third, the explicit inclusion of symmetry-equivalent reflections and systematic absences in the list of refined structure factors helps preserve the overall symmetry of the EDRMC configuration. Moreover, the incorporation of this restraint in the EDRMC refinement process helps ensure that the atomic displacements observed in the resultant configurations are as consistent as possible with the known average structure.

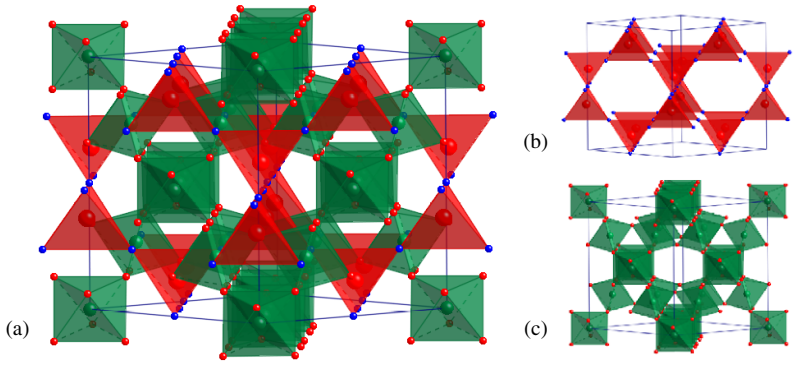

Figure 1. (a) Representation of the $[A_2O'][B_2O_6]$ pyrochlore structure in terms of its A_2O' and B_2O_6 subframeworks. (b) The A_2O' framework consists of a β-cristobalite-like array of corner-connected $[O'A_4]$ tetrahedra. (c) The B_2O_6 framework is assembled from corner-connected $[BO_6]$ octahedra.

3. Case study: $Bi_2Ru_2O_{7-\delta}$

3.1. Overview

As a preliminary test case for the EDRMC method, we chose to study the pyrochlore $Bi_2Ru_2O_{7-\delta}$. Bi-containing pyrochlores are known to exhibit a number of interesting physical properties; for example, both $Bi_2Ru_2O_{7-\delta}$ itself and the related $Bi_2Sn_2O_7$ show promise as electrocatalysts and as thin film resistors [32–36], Bi_2InNbO_7 is photocatalytic under UV radiation [37, 38] and the family $(Bi_{1.5}Zn_{0.5-\delta})(Zn_{0.5}Nb_{1.5})O_{7-\delta}$ has potential applications as resonators in high-frequency multilayer capacitors [39–41]. Perhaps unsurprisingly, a number of these materials are known to produce highly structured diffuse scattering patterns in electron diffraction experiments [40, 42, 43]. In this study, we present a number of electron diffraction diffuse scattering patterns for $Bi_2Ru_2O_{7-\delta}$ and proceed to refine atomistic models consistent with these patterns using EDRMC. We show that the observed scattering behaviour is due to correlated translations of Bi atoms within the structure.

The general pyrochlore structure, corresponding to the chemical formula $[A_2O'][B_2O_6]$, has $Fd\bar{3}m$ symmetry and can be considered in terms of two interpenetrating frameworks (figure 1): a β-cristobalite-like A_2O' network of corner-connected $[O'A_4]$ tetrahedra and a B_2O_6 array of corner-connected $[BO_6]$ octahedra. In the case of $Bi_2Ru_2O_{7-\delta}$, Bi atoms occupy the A site and Ru atoms the B site. Previous powder diffraction studies have shown that the material contains a small proportion of O′ vacancies [32, 44, 45], and in fact a neutron study suggested that Bi vacancies also occur, such that the overall composition is best given as $Bi_{1.89(1)}Ru_2O_{6.92(1)}$ [44]. We do not consider the issue of vacancy inclusion further in this study, employing instead the ideal composition $Bi_2Ru_2O_7$ for simplicity. Indeed we will show that the diffuse scattering patterns can be accounted for satisfactorily with this composition, and so it is unlikely that vacancy inclusion plays a significant role in the observed scattering behaviour.

What has emerged from the many average structure determinations of $Bi_2Ru_2O_{7-\delta}$ is that the Bi and O′ sites are characterized by abnormally large thermal parameters [32, 44–46]. In the case of the Bi site, the thermal motion is directed perpendicular to the coordinated $O'\cdots O'$ vector and is strongly anisotropic. A standard thermal ellipsoid does not model this disorder well; instead models involving split-atom sites have been proposed, and these have suggested a ‘doughnut’-like distribution of scattering density around this site [44, 45]. Chemically,

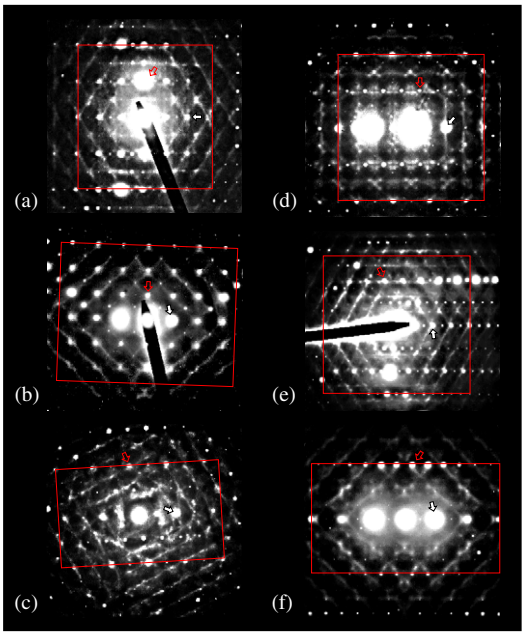

Figure 2. Typical EDPs obtained close to the (a) [11$\bar{2}$], (b) [001], (c) [$\bar{7}$12], (d) [$\bar{1}\bar{1}$8], (e) [21$\bar{3}$] and (f) [$\bar{1}$70] zone axes. The regions selected for use in EDRMC refinement are enclosed within the rectangles and were chosen because their reciprocal space coordinates could be determined easily from the indexed reflections. The reflections indicated respectively by the solid and open arrows are: (a) [$\bar{4}\bar{4}\bar{4}$]* and [$\bar{4}$40]*, (b) [400]* and [040]*, (c) [226]* and [08$\bar{4}$]*, (d) [4$\bar{4}$0]* and [531]*, (e) [444]* and [4$\bar{8}$0]*, (f) [004]* and [711]*.

this makes sense since bond valence calculations would suggest that the central O′ atom is significantly over-bonded ($V_{O'} = 2.8$); displacement of the average Bi position perpendicular to the O′–Bi–O′ vector acts to increase each of the O′–Bi bond lengths, helping to alleviate this situation.

Our approach in this study is to generate a single atomistic configuration that reflects at once both the *quantitative* constraints on mean squared displacements provided by average structure (Bragg) analysis and the *qualitative* local structure information reflected in the experimental diffuse scattering patterns. Through analysis of the correlations evident in this configuration, we hope to develop a semi-quantitative atomistic understanding of the underlying structural disorder in $Bi_2Ru_2O_{7-\delta}$.

3.2. Experimental

$Bi_2Ru_2O_{7-\delta}$ was prepared by the solid-state reaction of stoichiometric quantities of Bi_2O_3 (Aldrich) and Ru (Aldrich) as described previously [45]. The sample was ground into a fine powder and dispersed onto a holey carbon film for investigation using transmission electron microscopy (TEM). Electron diffraction patterns (EDPs) were obtained using a Philips EM 430 TEM.

3.3. Electron diffraction results

Figure 2 shows room temperature [11$\bar{2}$], [001], [$\bar{7}$12], [$\bar{1}\bar{1}$8], [21$\bar{3}$] and [$\bar{1}$70] zone axis EDPs. Structured diffuse scattering is clearly evident in each EDP and assumes the form of sheets

of diffuse intensity perpendicular to the six ⟨110⟩ directions of the average structure. This general motif is very similar in form to that characteristic of β-cristobalite [1, 47]. Quite apart from its overall periodicity, there are two informative features of this scattering distribution. First, the scattering is transverse polarised—the intensity of the observed diffuse streaking is strongest along directions of reciprocal space perpendicular to the streaking itself, and weakest (indeed absent) along directions parallel to the streaking. Consequently, the scattering arises from displacive rather than compositional disorder (e.g. vacancy ordering) [1]; moreover, the displacements responsible are both correlated and directed along the ⟨110⟩ directions (and uncorrelated along perpendicular directions). Second, the scattering—which in general terms runs across the $\langle hkl\rangle^* \pm \epsilon\langle h\bar{h}l\rangle^*$ regions of reciprocal space—obeys 'extinction conditions' such that, e.g. for diffuse scattering along $(1\bar{1}0)^*$, intensity is only observed whenever $h + k = 4n$. This implies that the relevant atoms are separated in real space by the vectors $\frac{1}{4}\langle 110\rangle$.

In β-cristobalite itself, the scattering behaviour is known to arise from concerted rotations of 'chains' of corner-connected $[SiO_4]$ tetrahedra, running along the ⟨110⟩ directions [47–50]. This form of motion indeed satisfies the requirements implied by the polarization and extinction conditions observed. The obvious analogy in $Bi_2Ru_2O_{7-\delta}$ would involve a similar regime of correlated rotations, but instead involving $[O'Bi_4]$ tetrahedra. We were interested to see whether this behaviour could be observed in EDRMC configurations refined against the diffuse scattering patterns.

3.4. EDRMC analysis

A configuration representing a $10 \times 10 \times 10$ supercell of the $Bi_2Ru_2O_7$ unit cell was prepared and each of the 88 000 atoms therein assigned small random displacements from their crystallographic positions. Before refining against the available electron diffraction data, the configuration was 'relaxed' using only the distance window constraint and structure factor restraint as implemented in EDRMC. This yielded an appropriate starting configuration with the correct average structure. The distance windows used were $1.4 \leqslant r_{Bi-O} \leqslant 3.5$ Å, $1.4 \leqslant r_{Bi-O'} \leqslant 3.5$ Å, $1.4 \leqslant r_{Ru-O} \leqslant 3.0$ Å and $2.2 \leqslant r_{O-O} \leqslant 3.5$ Å. The structure factor refinement included all reflections (hkl) such that $-8 \leqslant h, k, l \leqslant 8$, with expected structure factors calculated from the structural model termed 'Model 3' in [44]. Diffuse scattering patterns calculated from this initial configuration were completely featureless, as expected.

Suitable regions of each of the six EDPs shown in figure 2 were selected and prepared for use as input into the EDRMC program by excluding regions of Bragg scattering and the shadow image of the beam stop. Illustrations of the actual input data used are given in the left-hand panels of figure 3. An arbitrary acceptable standard deviation of five intensity units per pixel was applied for each of the six data sets (intensities being measured on a scale of 0 to 255). These diffuse scattering data were used in conjunction with the distance window constraint and the structure factor restraints (applied as above) to refine the EDRMC configuration as described in section 2. After approximately 48 h CPU time, the fits on the right-hand panels of figure 3 were obtained, without any significant change in the agreement between calculated and expected structure factors. The level of agreement obtained is clearly very satisfactory, and confirms that a single EDRMC configuration is capable of convincingly modelling a number of distinct experimental EDPs.

The configuration itself is shown in figure 4(a) and reveals that the refinement proceeded without incorporation of any large regions of 'damage' or other spurious atomic displacements. Visual inspection of the $O'Bi_2$ sub-framework reveals that the $[O'Bi_4]$ tetrahedra appear not to have been greatly distorted; moreover there is some evidence for the existence of β-cristobalite-like correlated rotations of these tetrahedra along ⟨110⟩ (figure 4(b)). However, it is possible

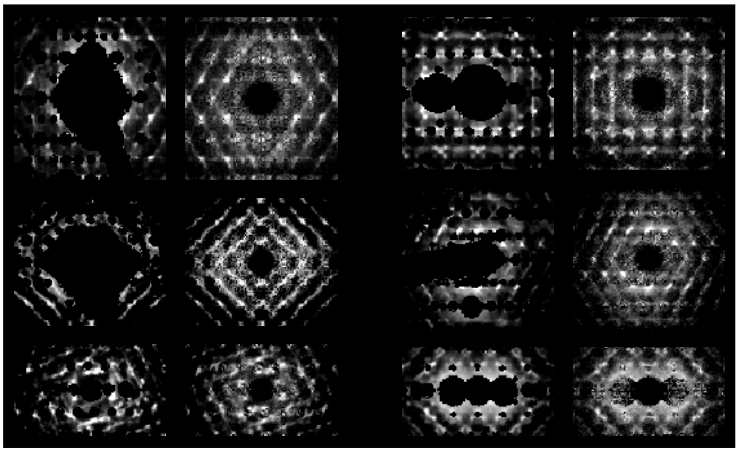

Figure 3. EDRMC electron diffraction input data (left-hand panels of the two columns) and refined fits (right-hand panels) for the regions of the experimental EDPs given in figure 2.

to analyse this configuration more systematically, and indeed one key advantage offered by a real-space configuration such as this is the ability to determine real-space distribution functions from the reciprocal-space diffraction data. Since—in this case—our diffraction data were fitted only qualitatively, the distribution functions will not be quantitatively accurate. However, since the refinement process was guided by (quantitative) structure factor restraints, one might expect to determine relative trends in the data with some degree of confidence.

Distance distribution functions for nearest-neighbour Ru–O, Bi–O′, Bi–O and Bi–Bi pairs were determined from our $Bi_2Ru_2O_7$ configuration and are given in figure 5(a). A number of comments may be made regarding these. First, all distributions appear reasonable; in particular, the absence of any truncation effects implies that the 'distance window' constraints used in the refinement process were not applied too constrictively. Second, the Ru–O and Bi–O′ distributions have similar widths, despite the large discrepancy in thermal parameters determined from the average structure. This confirms that the Bi/O′ displacements are indeed strongly correlated. Third, the Bi–Bi distribution is of comparable width to the nearest-neighbour Ru–O and Bi–O′ distributions—and much sharper than the Bi–O distribution. Despite the absence of any bonding interaction between Bi/Bi neighbours, their separation is preserved with a similar rigidity to that of nearest-neighbour ion pairs.

The distribution of Bi–O′–Bi angles within the same configuration is illustrated in figure 5(b), where it is also compared with that obtained from a configuration refined using only the average structure factor restraints. The average structures of both configurations are indistinguishable, but the configuration refined against the EDPs of figure 2 shows a significantly sharper angular distribution. Taken as a whole, these observations suggest that the geometry of individual [O′Bi_4] tetrahedra is tightly constrained in $Bi_2Ru_2O_{7-\delta}$ and resembles that of an ideal tetrahedron more strongly than the average structure demands.

A real-space 'scattering density' distribution can be obtained by collapsing the entire $10 \times 10 \times 10$ configuration onto a single unit cell (a portion of which is shown in figure 6(a)). This representation reveals that the Bi atoms are distributed throughout a flat disc-like region, rather than the 'doughnut' topology implicit in the structure factor restraints. This distribution is consistent with previous Monte Carlo simulations of cristobalite-like systems, where the superposition of tetrahedral-tilt modes across all ⟨110⟩ directions was shown to give similar

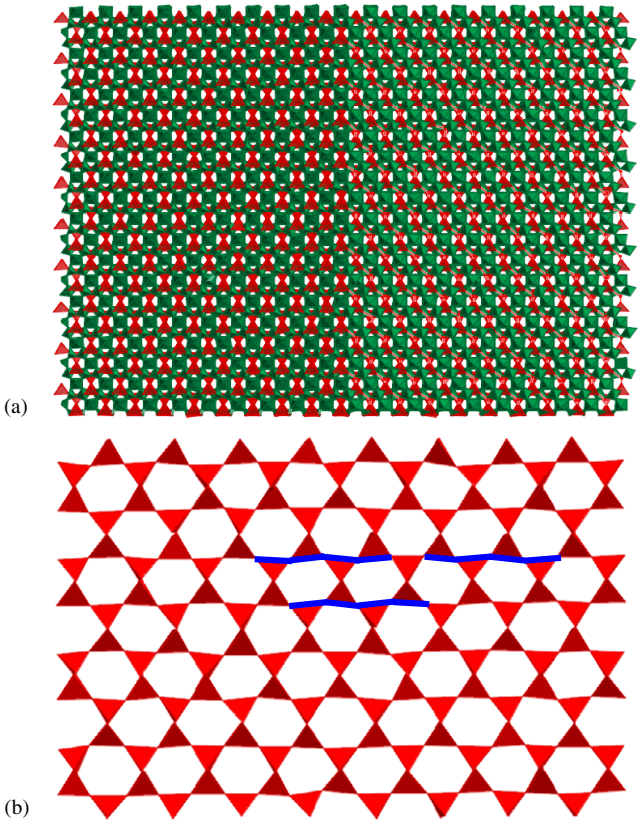

Figure 4. (a) Polyhedral representation of the EDRMC-refined $Bi_2Ru_2O_7$ configuration, corresponding to a $10 \times 10 \times 10$ supercell of the known crystallographic unit cell, viewed down the $[1\bar{1}0]$ crystal axis. (b) A small region of a $(1\bar{1}0)$ slice of the $O'Bi_2$ subframework in the configuration represented in terms of $[O'Bi_4]$ tetrahedra. Rigid unit mode-type tetrahedral-tilting displacements can be observed in several places (some examples are highlighted in bold).

disc-like distributions [40]. It is possible that this strongly anisotropic distribution is difficult to refine in powder diffraction analyses without the use of split-site models (which inherently produce 'doughnut'-shaped distributions).

Having established the various distributions implied by the electron diffraction images, we proceeded to investigate in greater detail the atomistic origin of the observed diffuse scattering patterns. What we are asking here is whether any explicit signature of the key atomic correlations responsible for the EDPs could be discerned from within the EDRMC configuration? Our approach is to calculate the set of Fourier displacement coefficients $T_{j\alpha}$ for each atom j and Cartesian axis α [12]:

$$T_{j\alpha}(\mathbf{k}) = \sqrt{\frac{m_j}{N}} \sum_{\ell} u_\alpha(j\ell) \exp[\mathrm{i}\mathbf{k} \cdot \mathbf{r}(j\ell)], \tag{12}$$

where m_j are the atomic masses and $u_\alpha(j\ell)$ the deviation of each atom from its average position $\mathbf{r}(j\ell)$. Then the sums

$$\varphi(j) = \sum_{\mathbf{k}\in\text{diffuse}} \sum_{\alpha} \left|T_{j\alpha}(\mathbf{k})\right|^2 \tag{13}$$

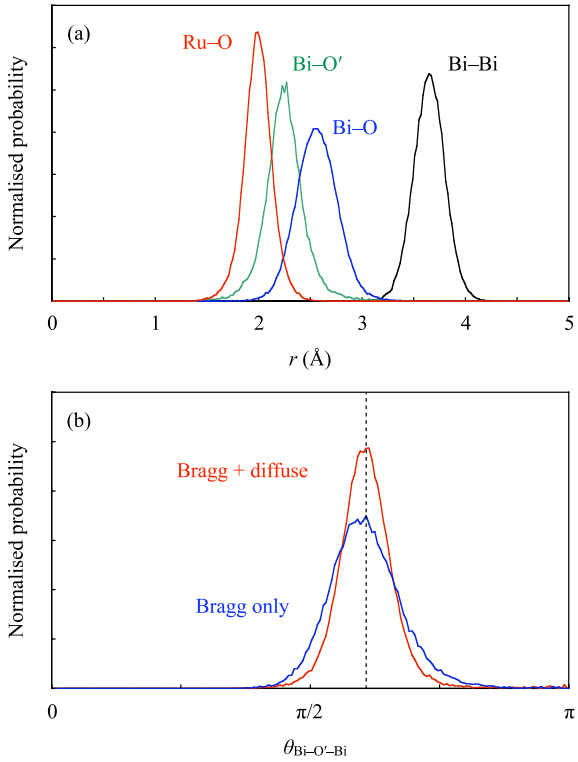

Figure 5. (a) Nearest-neighbour distance distribution functions extracted from the EDRMC $Bi_2Ru_2O_7$ configuration. (b) Intrapolyhedral Bi–O′–Bi bond angle distribution for an EDRMC configuration refined only against average structure factors and that obtained for the EDP/average-structure-refined EDRMC configuration. The dashed vertical line represents the ideal tetrahedral bond angle [$= \cos^{-1}\left(-\frac{1}{3}\right)$].

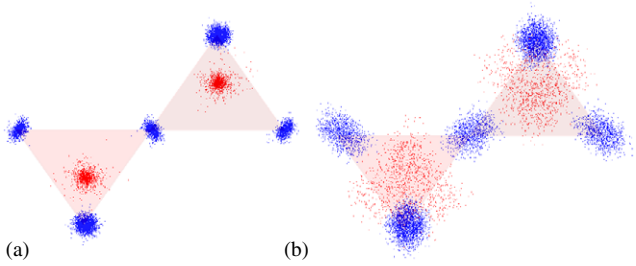

Figure 6. Scattering density distributions for a typical O'_2Bi_7 structural unit extracted from (a) EDP/average-structure-refined and (b) EDP/bond-valence-refined EDRMC configurations.

give mass-weighted 'participation coefficients' in the diffuse scattering for each atom. What these coefficients tell us is to what extent the motion of each atom is correlated along the wave-vectors associated with the diffuse scattering; the values calculated for each atom type are given in table 1. It is clear from this analysis that Bi displacements are indeed almost entirely responsible for the displacements from which the diffuse scattering patterns arise. We note that access to large numbers of independent configurations would allow calculation of both phonon

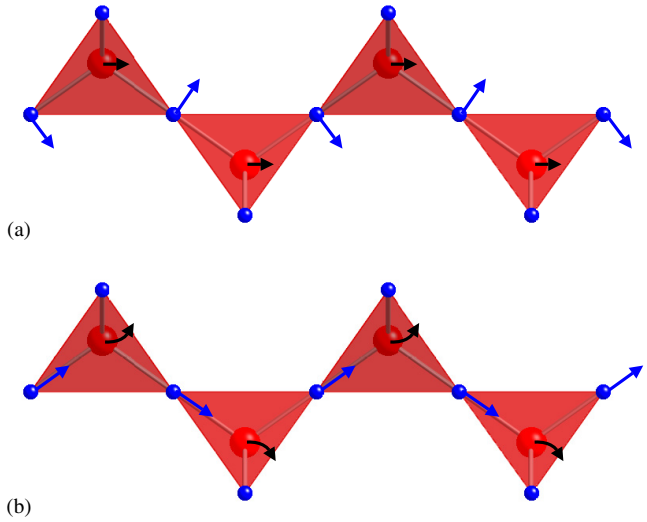

Figure 7. Correlated atomic displacement patterns derived from (a) EDP/average-structure-refined and (b) EDP/bond-valence-refined EDRMC configurations. In both cases the net Bi displacements occur parallel to the ⟨110⟩ axes, and are uncorrelated along perpendicular directions.

Table 1. Atomic diffuse scattering participation coefficients $\varphi(j)$ ($\times 10^{-45}$ kg m^2) calculated from the EDRMC configuration as described in the text.

j	Bi	Ru	O	O′
$\varphi(j)$	0.26(2)	0.017(4)	0.019(2)	0.030(2)

frequencies (which in this case will share the semi-quantitative nature of the diffuse scattering) and mode eigenvectors from the $T_{j\alpha}$ [12, 51]; however such an analysis is beyond the scope of this present investigation.

To summarize, what our EDRMC configuration has told us is that (i) the EDPs arise due to Bi translations correlated along the ⟨110⟩ directions, (ii) the [O′Bi$_4$] tetrahedra are rigid and (iii) the Bi displacements are normal to the O′ $\cdots$ O′ vectors. These observations are consistent only with a model in which the O′Bi$_2$ lattice supports a superposition of [O′Bi$_4$] tetrahedral-tilting modes of the sort illustrated in figure 7(a). These modes are direct analogues of the rigid unit modes (RUMs) found in β-cristobalite [52, 53], although it is of course impossible to determine whether the displacements in Bi$_2$Ru$_2$O$_{7-\delta}$ reflect static or dynamic disorder. The displacement pattern illustrated in figure 7(a) involves acentric translations of charged ions, and so will be associated with a change in dipole moment. Because the mode gives rise to observable EDPs, it is likely to be associated with a very low-frequency phonon mode (irrespective of whether the disorder in the native material is dynamic or static), and so may explain the ease with which a large net dipole moment can be supported in bulk samples.

We conclude our discussion of Bi$_2$Ru$_2$O$_{7-\delta}$ by considering the role played by bond valence constraints in the refinement process (these constraints were not employed in the analysis presented above). We found that very satisfactory fits to the experimental EDPs (comparable to those shown in figure 3) could be obtained by including bond valence restraints but excluding the average structure factor restraints. Despite reproducing the known diffuse scattering

Table 2. Average bond valence values calculated from $Bi_2Ru_2O_7$ EDRMC configurations. Standard deviations are given in parentheses.

Refinement strategy	Bi	Ru	O	O′
Average structure only[a]	3.7 (1.1)	4.4 (1.0)	2.2 (0.4)	3.2 (0.8)
EDPs and average structure	3.4 (0.7)	4.2 (0.6)	2.0 (0.3)	3.0 (0.5)
EDPs and bond valences	3.0 (0.2)	4.1 (0.2)	2.0 (0.2)	2.2 (0.2)

[a] Average bond valences determined from supercell configurations will generally be greater than the expected value as calculated from average atomic coordinates, since the latter neglects the effect of atomic displacements.

patterns, and indeed giving very favourable average bond valences across the configuration, the average structure observed in this second configuration was entirely inconsistent with the known Bragg intensity data. A scattering density distribution of part of the $O'Bi_2$ subframework is shown in figure 6(b), from which it is apparent that (i) the Bi displacements are oriented parallel to the average $O' \cdots O'$ vectors and (ii) the magnitude of the Bi and O′ displacements is unphysical.

In the absence of average structure data, the EDRMC procedure had arrived at a second possible solution to the diffuse scattering, based on the correlated displacements illustrated in figure 7(b). In this displacement pattern, the Bi and O′ atoms move primarily along the ⟨110⟩ directions in such a way that the distance between each O′ atom and three of its four coordinated Bi atoms remains constant, while the remaining O′–Bi bond length increases substantially. This has the effect of lowering the O′ bond valence significantly, while also effecting a minor decrease in that of the Bi atoms (table 2). Importantly, the displacements so produced do not affect the bond valence sums within other parallel chains of $[O'Bi_4]$ tetrahedra, and so are uncorrelated along directions perpendicular to the ⟨110⟩ axes.

While this second 'solution' gives highly distorted $[O'Bi_4]$ tetrahedra and clearly possesses the incorrect average structure, it does in fact produce a more reasonable ensemble of bond valences than the RUM-type configuration described initially (table 2). The intriguing question follows of why this particular displacement pattern is not found to occur in practice. What appears to be the case is that the very large displacements necessary to reduce bond valences to their ideal values act to bring non-bonded atom pairs into closer proximity than is physically reasonable; in particular a significant proportion of $Bi \cdots Bi$ pairs are separated by distances shorter than those observed in Bi metal. Consequently, we certainly do not believe that the bond-valence-driven EDRMC configuration represents a viable model of structural disorder in $Bi_2Ru_2O_{7-\delta}$. Nevertheless, it is of some interest that the same diffuse scattering patterns could be accounted for by a rather different—if not unrelated—set of correlated atomic displacements. Perhaps in other structurally related systems the balance between these two types of motion is less obvious; our results at least caution against the automatic interpretation of β-cristobalite-type EDPs in terms of RUMs alone.

We note that unphysical interatomic distributions may often be allowed in bond-valence-driven RMC simulations, given that the bond valence calculations do not constrain all atom types equally. In the case of $Bi_2Ru_2O_{7-\delta}$, there are no explicit constraints on the $Bi \cdots Bi$ separations; whereas the average structure factors will place quite definite limits on the spread of distances allowed. We did explore the possibility of employing *both* average structure *and* bond valence restraints within the same EDRMC refinement. This produced a continuous spectrum of configurations, where the particular bond valence σ_j and average structure factor $\sigma(hkl)$ values determined the extent to which the resulting solution resembled that obtained using either restraint by itself. Because we felt a compliance with the known average structure

was more meaningful in this case than the existence of 'correct' bond valence sums, we expect the average structure factor refinement produced the more physically realistic structural model.

4. Summary and conclusions

What our study has achieved is to illustrate that the reverse Monte Carlo method can be successfully used to refine atomistic configurations consistent with experimentally observed EDPs. As described, the approach provides a semi-quantitative method for extracting real-space distributions from these EDPs, yielding valuable insight into local structure otherwise unobtainable from average structure analysis alone. Because electron diffraction is a routine method capable of being used with polycrystalline samples, there is significant scope for application to a range of materials with unusual physical properties.

We have also identified a general need for caution when applying constraints/restraints to the EDRMC refinement process. In particular, while bond valence sums are widely used as a means of understanding disorder in crystalline materials, we found that a bond-valence-driven refinement of $Bi_2Ru_2O_{7-\delta}$ EDPs gave a spurious solution to the data. Instead, restraining the average structure of the EDRMC configuration to match that obtained from Rietveld refinement gave what we believe to be the correct structural interpretation of displacive disorder in the material. This is not to say that bond valence restraints will be inappropriate for EDRMC studies in general; however, care should be taken to ensure their use does not jeopardise the ability to reproduce experimental data. We note that the use of bond valence sums to identify likely mechanisms of disorder from average structure solutions (e.g. as used in [43, 54]) differs fundamentally from their application as local structure restraints in atomistic simulations such as RMC. Precisely how this difference would be reflected in the structural models so obtained is by no means obvious. What is known is that the available bond valence parameters are calculated from average structure refinements [29, 30], and so the extension to atomistic configurations may not follow automatically.

The inclusion of additional data-based restraints on the refinement process would be expected to substantially improve the quality of the models obtained. In this respect, the parallel refinement of EDPs with, for example, powder neutron and/or x-ray diffraction data is an obvious future direction for expansion of the EDRMC method. There will also be instances where the incorporation of geometric restraints—additional χ^2 terms which act to favour ideal coordination polyhedral geometries—would produce yet more realistic structural models. Nevertheless, this work has helped establish that real-space analysis of electron diffraction data is a viable analytical tool and can yield valuable new information when studying structural disorder in crystalline materials.

Acknowledgments

The authors thank B Kennedy (University of Sydney) for supplying the $Bi_2Ru_2O_{7-\delta}$ sample used in this study. ALG is grateful to Trinity College, Cambridge for a Research Fellowship, and to the Research School of Chemistry, Australian National University for a Visiting Fellowship. RLW and H-BN thank the Australian Research Council for funding in the form of an ARC Discovery Grant.

References

[1] Withers R L 2005 *Z. Kristallogr.* **220** 1027
[2] Borie B and Sparks C J 1971 *Acta Crystallogr.* A **27** 198

[3] Wu T B, Matsubara E and Cohen J B 1983 *J. Appl. Crystallogr.* **16** 407
[4] Welberry T R and Butler B D 1994 *J. Appl. Crystallogr.* **27** 205
[5] Krivoglaz M A 1969 *The Theory of X-ray and Thermal Neutron Scattering by Real Crystals* (New York: Plenum)
[6] de Fontaine D 1972 *J. Phys. Chem. Solids* **33** 297
[7] Pèrez-Mato J M, Madariaga G, Zuniga F J and Garcia Arribas A 1987 *Acta Crystallogr.* A **43** 216
[8] Dagotto E 1994 *Rev. Mod. Phys.* **66** 763
[9] Dagotto E, Hotta T and Moreo A 2001 *Phys. Rep.* **344** 1
[10] Nield V M, Keen D A, Hayes W and McGreevy R L 1993 *Solid State Ion.* **66** 247
[11] Evans J S O 1999 *J. Chem. Soc.: Dalton Trans.* 3317
[12] Dove M T 1993 *Introduction to Lattice Dynamics* (Cambridge: Cambridge University Press)
[13] Salje E K H 1990 *Phase Transitions in Ferroelectrics, Ferroelastic and Co-elastic Crystals* (Cambridge: Cambridge University Press)
[14] Soper A K 2005 *Phys. Rev.* B **72** 104204
[15] Welberry T R, Proffen Th and Bown M 1998 *Acta Crystallogr.* A **54** 661
[16] McGreevy R L and Pusztai L 1988 *Mol. Simul.* **1** 359
[17] Nield V M, Keen D A and McGreevy R L 1995 *Acta Crystallogr.* A **51** 763
[18] Welberry T R and Proffen Th 1998 *J. Appl. Crystallogr.* **31** 309
[19] Proffen Th and Welberry T R 1998 *J. Appl. Crystallogr.* **31** 318
[20] Proffen Th 1998 *Physica* B **241–243** 281
[21] McKenzie D R, Davis C A, Cockayne D J H, Muller D A and Cassallo A M 1992 *Nature* **355** 622
[22] Mellergård A and McGreevy R L 1999 *Acta Crystallogr.* A **55** 783
[23] Mellergård A and McGreevy R L 2000 *Chem. Phys.* **261** 267
[24] Tucker M G, Keen D A, Dove M T, Goodwin A L and Hui Q 2007 *J. Phys.: Condens. Matter* **19** 335218
[25] Evrard G and Pusztai L 2005 *J. Phys.: Condens. Matter* **17** S1
[26] Butler B D and Welberry T R 1992 *J. Appl. Crystallogr.* **25** 391
[27] Goodwin A L, Tucker M G, Cope E R, Dove M T and Keen D A 2005 *Phys. Rev.* B **72** 214304
[28] Brown I D 1981 *Structure and Bonding in Crystals* vol 2, ed M O'Keeffe and A Navrotsky (New York: Academic) pp 1–30
[29] O'Keeffe M 1989 *Struct. Bonding (Berlin)* **71** 162
[30] Brese N E and O'Keeffe M 1991 *Acta Crystallogr.* B **47** 192
[31] Tucker M G, Dove M T and Keen D A 2001 *J. Appl. Crystallogr.* **34** 780
[32] Facer G, Elcombe M M and Kennedy B J 1993 *Aust. J. Chem.* **46** 1987
[33] Beyerlein R A, Horowitz H S, Longo J M, Leonowicz M E, Jorgensen J D and Rotella F J 1984 *J. Solid State Chem.* **51** 253
[34] Radosavljevic I, Evans J S O and Sleight A W 1998 *J. Solid State Chem.* **136** 63
[35] Jones R H and Knight K S 1997 *J. Chem. Soc.: Dalton Trans.* 2551
[36] Radosavljevic Evans I, Howard J A K and Evans J S O 2003 *J. Mater. Chem.* **13** 2098
[37] Zou Z, Ye J and Arakawa H 2000 *Solid State Commun.* **116** 259
[38] Zou Z G, Ye J H, Abe R and Arakawa H 2000 *Catal. Lett.* **68** 235
[39] Mergen A and Lee W E 1997 *Mater. Res. Bull.* **32** 175
[40] Withers R L, Welberry T R, Larsson A-K, Liu Y, Norén L, Rundlöf H and Brink F J 2004 *J. Solid State Chem.* **177** 231
[41] Levin I, Amos T G, Nino J C, Vanderah T A, Randall C A and Lanagan M T 2002 *J. Solid State Chem.* **168** 69
[42] Zhou Q, Kennedy B J, Ting V and Withers R L 2005 *J. Solid State Chem.* **178** 1575
[43] Liu Y, Withers R L, Welberry T R, Wang H and Du H 2006 *J. Solid State Chem.* **179** 2141
[44] Avdeev M, Hass M K, Jorgensen J D and Cava R J 2002 *J. Solid State Chem.* **169** 24
[45] Li L and Kennedy B J 2003 *Chem. Mater.* **15** 4060
[46] Abraham F, Nowogrocki G and Thomas D 1975 *C. R. Acad. Sci. Fr.* C **279** 279
[47] Hua G L, Welberry T R, Withers R L and Thompson J G 1988 *J. Appl. Crystallogr.* **21** 458
[48] Welberry T R, Hua G L and Withers R L 1989 *J. Appl. Crystallogr.* **22** 87
[49] Swainson I P and Dove M T 1993 *Phys. Rev. Lett.* **71** 193
[50] Tucker M G, Squires M P, Dove M T and Keen D A 2001 *J. Phys.: Condens. Matter* **13** 403
[51] Goodwin A L, Tucker M G, Dove M T and Keen D A 2004 *Phys. Rev. Lett.* **93** 075502
[52] Dove M T, Giddy A P and Heine V 1992 *Ferroelectrics* **136** 33
[53] Giddy A P, Dove M T, Pawley G S and Heine V 1993 *Acta Crystallogr.* A **49** 697
[54] Welberry T R, Gutmann M J, Woo H, Goossens D J, Xu G, Stock C, Chen W and Ye Z-G 2005 *J. Appl. Crystallogr.* **38** 639